Nanoscale

PAPER

View Article Online
View Journal | View Issue

Cite this: *Nanoscale*, 2014, **6**, 1064

Dynamic nanocrystal response and high temperature growth of carbon nanotube–ferroelectric hybrid nanostructure†

Ashok Kumar,*[a] J. F. Scott[bc] and R. S. Katiyar[b]

Received 24th July 2013
Accepted 18th October 2013

DOI: 10.1039/c3nr03811d

www.rsc.org/nanoscale

A long standing problem related to the capping of carbon nanotubes (CNT) by inorganic materials at high temperature has been solved. *In situ* dynamic response of $Pb(Zr_{0.52}Ti_{0.48})O_3$ (PZT) nanocrystals attached to the wings of the outer surface of PZT/CNT hybrid-nanostructure has been demonstrated under a constant-energy high-resolution transmission electron microscopy (HRTEM) e-beam. PZT nanocrystals revealed that the crystal orientations, positions, faces, and hopping states change with time. HRTEM study has been performed to investigate the microstructure of hybrid nanostructures and nanosize polycrystal trapped across the wings. Raman spectroscopy was utilized to investigate the local structures, defects, crystal qualities and temperature dependent growth and degradation of hybrid nanostructures. Raman spectra indicate that MWCNT and PZT/MWCNT/n-Si possess good quality of CNT before and after PZT deposition until 650 °C. The monoclinic *Cc*/*Cm* phase of PZT which is optimum in piezoelectric properties was prominent in the hybrid structure and should be useful for device applications. An unusual hexagonal faceting oscillation of the nano-crystal perimeter on a 10–30 s period is also observed.

Introduction

In this decade, controlled inorganic–organic hybrid nanostructures have been one of the promising topics for interdisciplinary research.[1] Organic carbon nanotubes and graphene have a special advantage as interconnects. Moore's law predicts doubling of transistors on the chip every 18 months through size reduction.[2–4] Until now this target has been valid, but it is facing fundamental quantum mechanical atomic limits. Two possible solutions are three dimensional (3D) nanostructures and quantum computing; the first option is extremely useful for the vertical integration of devices with a low operating voltage, moderate heat exhaust and relatively very high matrix density.[5] In the present manuscript we solve some basic nanoscale integration problems: Five years ago, some of the present authors were the first to integrate ferroelectric nano-actuators and nano-transducers onto carbon nanotube interconnects[6] using techniques that are also applicable to ZnO nano-devices. However, the processing temperature windows were extremely narrow. Put simply, ferroelectric oxides require a high-temperature growth in oxygen, and under these conditions carbon nanotubes can ignite. In a more recent work[7] we have greatly extended the processing temperature range. In the present work we examine the dynamics of the nano-ferroelectrics that form functional end groups on the multiwalled carbon nanotubes.

Several discoveries on CNT and graphene have changed the orientation of organic science research.[8,9] Highly mechanical, thermal, electrical, transport, corrosion-resistant, optical properties and easy integration with organic–inorganic devices make carbon nanotubes (CNT) and graphene potential candidates for future high speed transistors, touch screen panels, solar cells, sensors, and other applications.[10] Similarly, $Pb(Zr_{1-x},Ti_x)O_3$ (PZT) is a well known ferroelectric/piezoelectric material with robust functional properties for the non-volatile random access memory (NVRAM), and sensor and actuator applications.[11] Both systems have some merits and demerits for the next generation device elements. To overcome these limitations, a new inorganic–organic hybrid nanostructures approach has been proposed for the next generation memory elements.[7]

The dynamic behavior of gases, liquids and solids was studied in the context of its movement across the channel of MWCNT.[12–16] The movement of water droplets across the inner cavity of the CNTs due to the capillary forces has been observed, but it is feasible only if the surface tension of the filling liquid is below the cut-off value of 100–200 mN m^{-1}.[12] Kumar *et al.* report the movement of liquid indium metal inside the indium oxide nanotubes in the presence of an energetic e-beam; however, the main reason for such action was the generated heat from

[a]*CSIR-National Physical Laboratory, K. S. Krishnan Marg, New Delhi 110012, India. E-mail: ashok553@nplindia.org*

[b]*Department of Physics and Institute for Functional Nanomaterials, University of Puerto Rico, San Juan, PR 00931-3334, USA*

[c]*Department of Physics, Cavendish Laboratory, University of Cambridge, Cambridge CB3 OHE, UK*

† Electronic supplementary information (ESI) available. See DOI: 10.1039/c3nr03811d

e-beam solid interaction.[13] They also observed real time rocket type propulsion in the metal filled indium oxide.[14] Knechtel *et al.* showed the reversible bending of carbon nanotubes with change in the current density of irradiated e-beam of transmission electron microscope.[15] Bhattacharyya *et al.* proposed a realistic model for the elastic stretching of MWCNT under such an energetic irradiated e-beam.[16] Recent work suggests that electron beam irradiation elevates both temperature and pressure and a complex phase of inorganic, organic and hybrid nanostructures.

Another question is the existence of CNTs at high temperature and ambient oxygen atmosphere, where CNTs can simply burn under such conditions. The capping of MWCNT by thin polar ferroelectric films is a delicate process, because oxide ferroelectrics require high-temperature deposition in oxygen ambient. Fabrication and switching properties of polycrystalline $Pb(Zr_{0.52}Ti_{0.48})O_3$ (PZT)/MWCNT/n-Si nanostructures have already been reported elsewhere.[7] This report presents the dynamic behavior of PZT nanocrystals grown on aligned MWCNT hybrid nanostructure by irradiation of an e-beam. Microstructure–property relation and sustainability of hybrid nanostructures are discussed below as a function of growth temperatures using multipurpose Raman spectroscopy.

Experimental

The synthesis and growth mechanism of the PZT/MWCNT/n-Si nanostructures have been discussed elsewhere.[7] Arrays with controlled pitch, dimension, and height, and good registration of the MWCNTs were obtained on the n-Si by plasma enhanced chemical vapor deposition (PECVD) techniques.[17] Acetylene (C_2H_2) (for CNT growth) and ammonia (NH_3) (to etch the unwanted amorphous carbon) gases were used for growth of MWCNT at 700 °C at ambient conditions. Thin ferroelectric $Pb(Zr_{0.52}Ti_{0.48})O_3$ (PZT) films were coated on the aligned MWCNT by a pulsed laser deposition (PLD) technique.[18] Low laser repetition rate (5–7 Hz), moderate laser energies (1–2 J cm^{-2}), low oxygen atmospheres (70–80 mTorr), and a large temperature range (500–700 °C) were employed to obtain high quality crystalline films on MWCNT utilizing a KrF Excimer laser (λ = 240 nm). Post PZT deposition, the chamber was cooled at a rate of 10 K min^{-1} up to 300 °C and subsequently 5 K min^{-1} until room temperature in an oxygen atmosphere at 300 Torr. The microstructure of PZT/MWCNT was studied with high resolution transmission electron microscopy with a Cs probe corrected JEOL JEM-2200FS TEM. A scanning tunneling electron microscopy (STEM) mode was used for the cross-sectional analysis of individual hybrid nanotubes. Raman spectra of MWCNT were obtained in a backscattering configuration using a double-grating Jobin Yvon T64000 spectrometer (gratings with 1800 grooves per mm) operating in subtractive mode. A coherent argon ion laser (Innova 90-5) with 10 mW power of vertically polarized green laser light lasing at 514.5 nm was used to collect the phonon spectra. A liquid-nitrogen-cooled CCD device collected the Raman scattered signal through an 80× objective. The spectra were peak-fitted with Lorentzian function after linear background corrections. Piezo force microscopy (PFM) study was carried out on a commercially available atomic force microscope (Asylum, MFP-3D). Bias-off PFM local switching loops were obtained as a function of dc switching pulses superimposed on ac modulation bias. A typical frequency range for an ac voltage was 300–350 kHz with an amplitude of 0.8 V (peak-to-peak).

Results and discussion

Fig. 1(a)–(f) show a TEM image of single PZT/MWCNT nanotube grown at 600 °C which was extracted from the well defined registered array fabricated on n type silicon. Fig. 1(f) is a schematic drawing to clarify the membrane position shown in Fig. 1(a)–(c). Fig. 1(d) and (e) represent the sea of ultrafine PZT nano-crystals and outer cage of nanocrystals, respectively. The microstructure presented here is a representation of all the PZT/MWCNT grown over a wide range of temperatures. In most deposition conditions these MWCNTs were sustained until 650 °C; above this temperature CNTs started degrading, depending upon the growth time and oxygen partial pressure. Ajayan *et al.*[19] demonstrate the detailed oxidation conditions of MWCNT with temperatures and oxygen partial pressures. Oxidation starts rapidly above 700 °C with peeling off the outer graphene layer by layer; resulting in the thinning of the MWCNTs. Microstructures revealed that these PZT crystals are conformal over the MWCNTs from head to tail, although in some cases these coating are non-uniform with a thicker portion at the end cap as compared to the base (near the silicon substrates). A similar phenomenon was observed for all cases, whether the MWCNT was a dense forest or a well defined registered array.

Fig. 1(a)–(e) presents the different microstructural aspects of a single PZT/MWCNTs hybrid nanotube detached from the array of PZT/MWCNTs/n-Si. In general, the diameter of MWCNT is around 80 (±10) nm, conformally covered by a 50 to 80 nm PZT layer, depending on the wall strength and adhesion. A large number of polycrystalline nanosized PZT crystals of average diameter 2–5 nm were trapped across the wings of the PZT top surface formed during the growth. These nanocrystals hopped in a sea of ultrafine membranes formed across the wings under constant electron beam energy. The diffraction patterns of these nanocrystals are shown in the inset of Fig. 1(a) and the distance between the (111) plane is 2.355 Å, implying a polycrystalline nature and a good match with the crystal structure of ultra-thin PZT films. The dynamic behavior of these crystals is reminiscent of the swinging of solid nanoparticles in liquid medium under irradiation of energetic e-beams. There might be two basic reasons; (i) production of localized heat by e-beams during the microstructure study which in turn changes the crystal orientations and movements and may be sometimes their crystallographic phases, (ii) energy gain by the nanocrystals during the interaction of energetic e-beam which in turn changes the crystal position and crystallographic face. In order to avoid any artifacts in the microstructural study, HRTEM was operated at a very high voltage in order to minimize the damage rate due to Bethe–Bloch cross-section for electron–electron interaction.[20] Fig. 1(d) demonstrates the large sea of

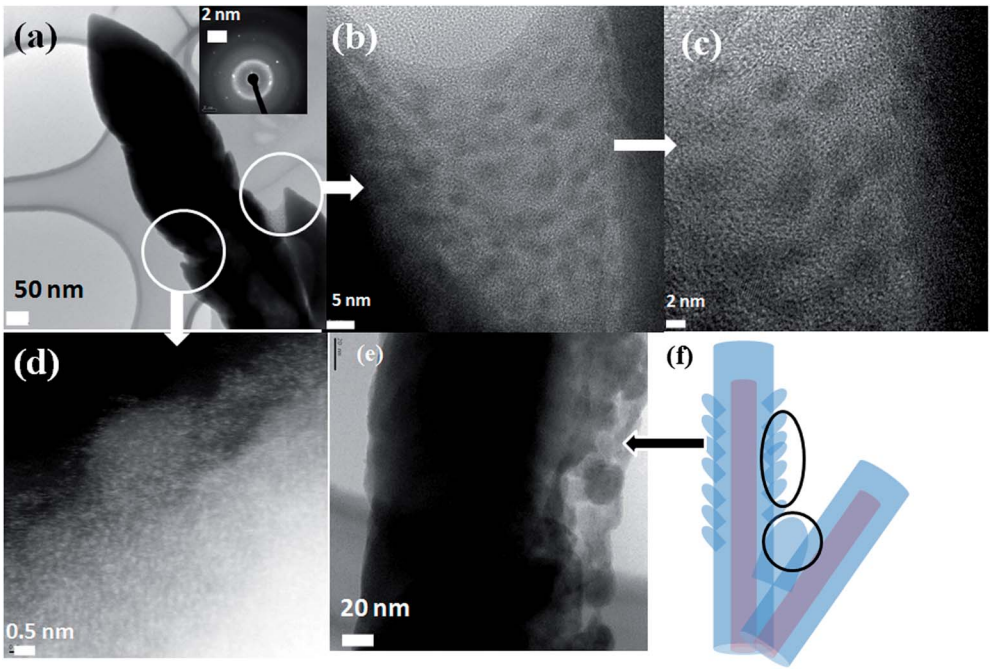

Fig. 1 (a) Dark field STEM image of the single PZT/MWCNT nanotubes scraped from the registered array nanostructure (bar scale 50 nm), (b) HRTEM image of the trapped PZT nanoparticles at the edge of the hybrid structure (5 nm bar scale), (c) trapped PZT crystal (2 nm), (d) ultrafine PZT nanocrystals in the fence of the membranes form across the wings (0.5 nm bar scale), (e) cage and edge of oscillating/hopping nanoparticles in the matrix (bar scale 20 nm), (f) schematic diagram of PZT/MWCN nanostructure (black circles indicate cage and edge of trapped PZT nanocrystals).

nanocrystals in the membranes. Fig. 1(a)–(e) shows the trapped nanocrystals in the membranes, well separated from each other in an amorphous matrix. However, this microstructure was only seen near the outer edge and between the wings of the hybrid nanostructure. Capping of ultrathin PZT (<5–7 nm) film is needed for the study of interior and interface between the PZT and MWCNT.

Fig. 2(a)–(d) shows the *in situ* microstructure of the same area of the nanocrystals under similar e-beams energy at different times. A steady e-beam was irradiated at 30 s intervals to check the crystal morphology at the nanoscale; interestingly, these nanocrystals display a dynamic response. It seems that the nanocrystal positions, crystallographic planes, and orientations change with irradiation energy and probing time. The changes in the positions and planes are not controlled and systematic, but depend on the site and occupancy of the crystal. *In situ* dynamic response shows hopping of nanocrystals due to the interaction with the e-beam. This is the first time we have seen such behavior of nanocrystals bonded in a solid matrix. These observations suggest the spatial variation may be due to change in the localized energy due to interaction of the energetic e-beams with nanocrystals. Another possible reason is that the conducting MWCNTs may act as one electrode allowing charging due to irradiation of the e-beam to be grounded. The resulting mechanical shock for piezoelectric nano-crystals may be responsible for the temporal and spatial variation. Further study is required for the real causes and physics behind this phenomenon. We note that, in addition to the dramatic changes in ferroelectric domains and domain walls inside the PZT target, faceting develops and disappears at the perimeter of the nano-crystals on a 10–30 s period. This is also of interest: two-dimensional thin films have one-dimensional perimeters,

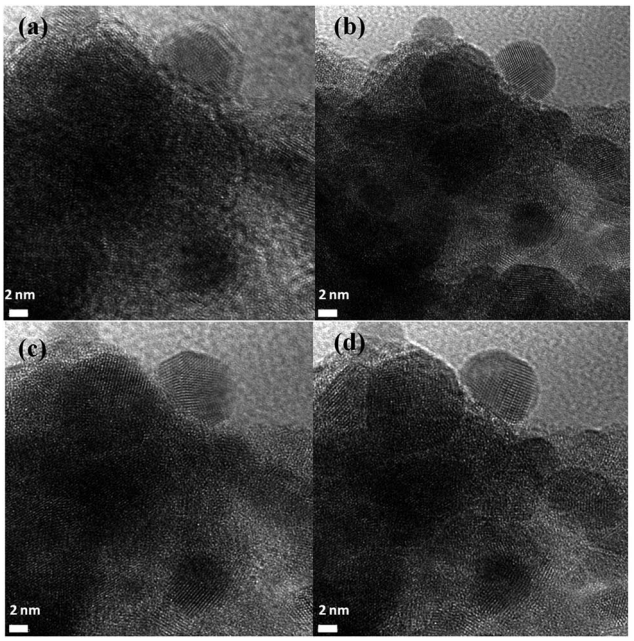

Fig. 2 (a) HRTEM image of hopping PZT nano-particles, nanocrystals plane, orientation, hopping effect (a) first image (0 second), (b) 30 second, (c) 60 second, (d) 90 second, position and beam energy were constant during the investigation.

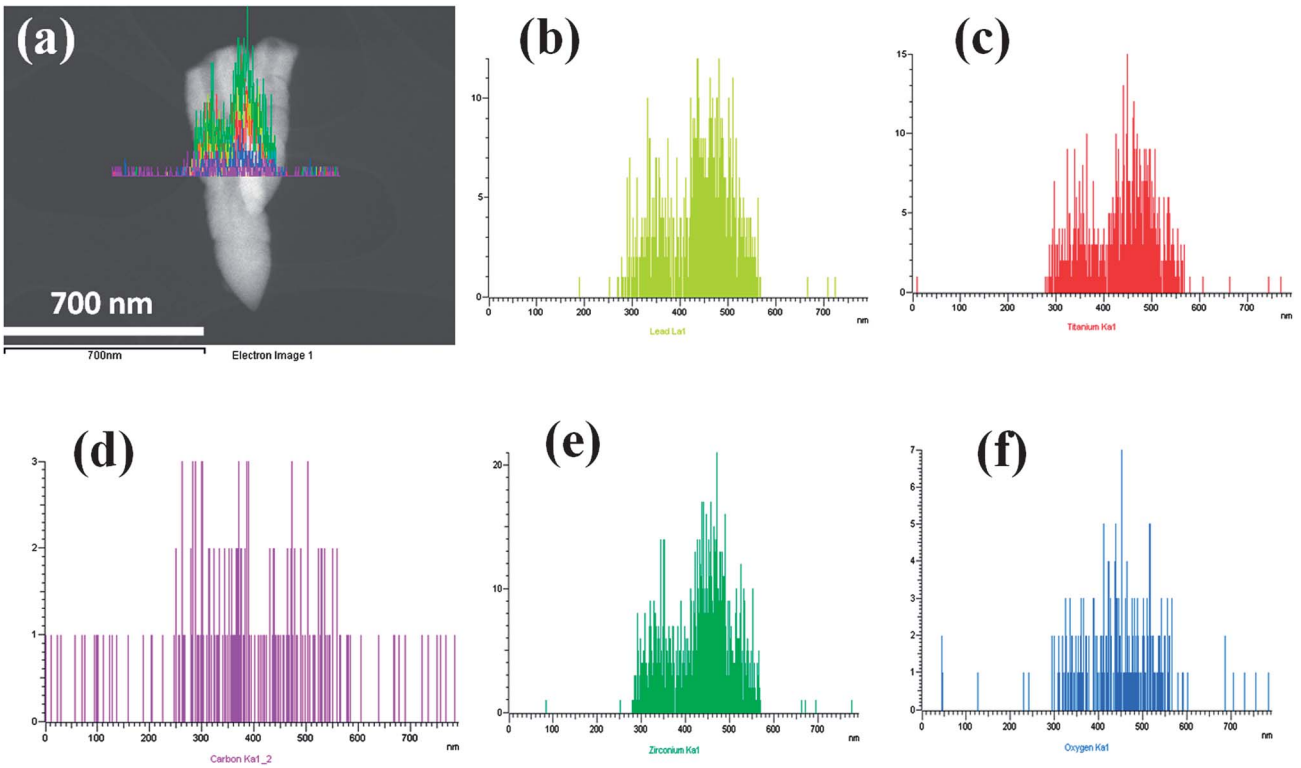

Fig. 3 (a) STEM image of the single PZT/MWCNT nanotubes, compositional mapping of (b) lead, (c) titanium, (d) carbon, (e) zirconium, and (f) oxygen.

and one-dimensional parameters cannot change the length in thermal equilibrium. Such faceting in nano-crystals is well known during crystal growth, but can also occur during ferroelectric switching, which is also non-equilibrium. Faceting oscillations have not been reported before in ferroelectric nanocrystals.

Fig. 3(a)–(f) shows a cross-sectional scanning transmission electron microscopy (STEM) image and the compositional mapping of each element. The energy-dispersive X-ray spectroscopy (EDX) and mapping demonstrate that these deposited films possess quite close compositions to the target used for deposition. The intensity of all compositions is quite high except for the carbon. The weak intensity of the carbon is quite obvious: in order to check the carbon contents of the nanotubes one should study the ultra-thin film-coated MWCNTs, which would be easy to penetrate by e-beams. It also indicates that the shape of the MWCNTs has clearly been preserved despite thick PZT coating on the top of the MWCNTs. As discussed, these aligned MWCNTs were grown by utilizing a Ni catalyst, and hence Ni was sitting on the top of the tubes. These nanotubes were also facing towards the plume generated by PLD, which favors the formation of a thick PZT layer at the top of hybrid nanostructures. Chemical inhomogeneities in the microstructure were also evident from the presence of relaxor ferroelectric F_{2g} modes (not soft, and implying the localization of Pb–O bonding).[21]

Fig. 4 shows the Raman spectra of PZT/MWCNT/n-Si nanostructures grown at various temperatures. As-grown MWCNTs have two prominent peaks at high frequency around 1355 cm^{-1}

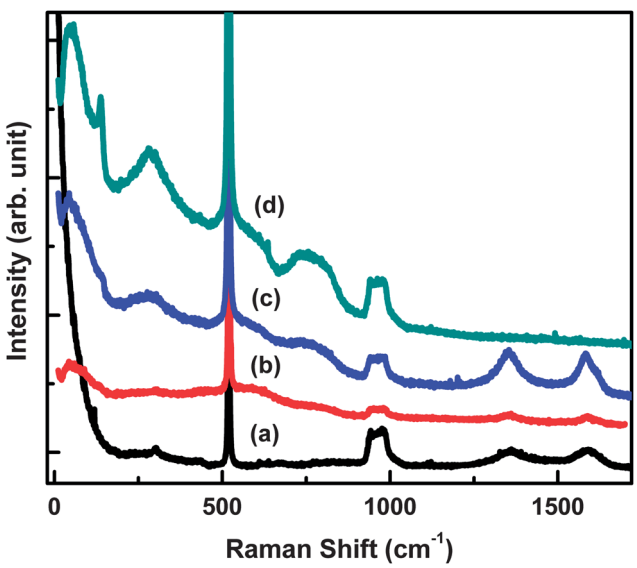

Fig. 4 Raman spectra of the registered array of PZT/MWCNT/n-Si nanotubes (a) as grown MWCNT/n-Si, (b) after PZT deposition at 500 °C, (c) after PZT deposition at 600 °C, and (d) after PZT deposition at 700 °C.

(D band) and 1588 cm^{-1} (G band) due to disordered graphitic carbon structures. The low-frequency defect peak (D band) positions varied over 10–15 cm^{-1}, depending on the quality of walls and nanotubes and their growth conditions. Their intensities also changed from sample to sample. Raman spectroscopy is a versatile tool to detect the defects in a crystal structure

and investigate the local microstructure of micro/nano-crystalline systems. Large background Si Raman spectra were also observed with some extra peaks due to processing of the catalyst and lithography for the formation of aligned MWCNTs.

High frequency Raman spectra of the PZT/MWCNT/n-Si are analyzed using the damped harmonic oscillator model (DHO).[22] The observed vibrational modes are analyzed and fitted with the spectral response function.

$$S(\nu) = \sum_i \frac{\chi_{0i}\Gamma_i\nu_{0i}^2\nu}{(\nu^2 - \nu_{0i}^2) + \Gamma_i^2\nu^2}F(\nu, T) \quad (1)$$

where $F(\nu,T) = [n(\nu) + 1]$ (Stokes scattering) and $n(\nu) = [\exp(h\nu/\kappa T) - 1]^{-1}$. The parameters in eqn (1) amplitude χ_0 (in arbitrary units), the mode frequency ν_0, the damping constant Γ, and the temperature T, describe each phonon mode as a damped harmonic oscillator.

Two well-defined MWCNTs peaks at 1588–1583 cm^{-1} and 1365–1355 cm^{-1} could be assigned to the fundamental frequency modes E_{2g} and D (induced by defects) analogous to those of graphite.[23] The above phonon function (eqn (1)) is used for modes fitting and presented in Fig. 5. The intensity of defect mode (D band) increased as compared to the G band with the increase in deposition temperature, implying the degradation of the upper surface of MWCNT at elevated growth temperatures. Generally good quality MWCNTs do not oxidize until 650 °C as can be seen from Fig. 4 and 5. Fig. 4(d) shows absence of both MWCNTs modes grown at 700 °C, however, sometimes one can see well defined high frequency Raman spectra, even the hybrid structure grown at 700 °C. It mainly depends on CNT quality and growth parameters (oxygen, temperature, and pressure).

PZT is a well-investigated system, and its Raman analysis is well understood for the different compositional ratios of Zr/Ti. T-rich PZT has a tetragonal crystal structure with *P4mm* space group.[24] Assignment of Raman active modes near the morphotropic phase boundary (MPB) is an unfinished research work and depends on the crystal quality. Noheda *et al.* found the monoclinic phase (*Cm* space group) with 12 Raman modes near the MPB ($0.45 < x < 0.66$) which was considered as a derivative of both tetragonal and rhombohedral phases.[22,25] Fig. 4 indicates a prominent low frequency Raman mode at ~48 cm^{-1} which agrees with the monoclinic phase of PZT near MPB observed by Lima *et al.* It is similar to the low lying F_{2g} mode of relaxor ferroelectric as observed in many lead based classical relaxors.[19] Note that the F_{2g} mode appears due to the compositional inhomogeneity and development of nanoscale polar regions in the matrix. HRTEM images show the presence of very fine 2–4 nm PZT beads embedded in the cage of the outer surface of PZT; these support the F_{2g} mode. Three-dimensional stress due to the heavy load of PZT on MWCNT may also be responsible for this low-lying phonon mode. The other Raman-active modes of PZT are dominated by sharp n-Si substrate peaks in the same regions; however, significant enhancement in the intensity of phonon modes lying between 200 and 300 cm^{-1} can be seen after the PZT deposition, which increases with increase in the crystallinity and growth temperature. At 700 °C, all the low-lying PZT Raman modes were sharp; yet the mode assignment is not precise due to the high background of the substrate and the polycrystalline nature of the films. Raman spectra authenticate the formation of monoclinic PZT and fabrication of PZT/MWCNT/n-Si up to 650 °C, which degrade at elevated

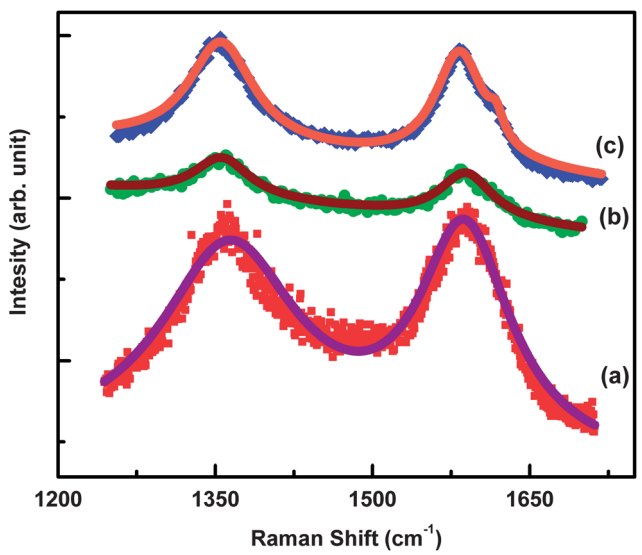

Fig. 5 High frequency MWCNT nanotube modes and their fitting with DHO function, phonon behavior with different PZT coating temperatures (a) as grown CNT, (b) at 500 °C, (c) at 600 °C.

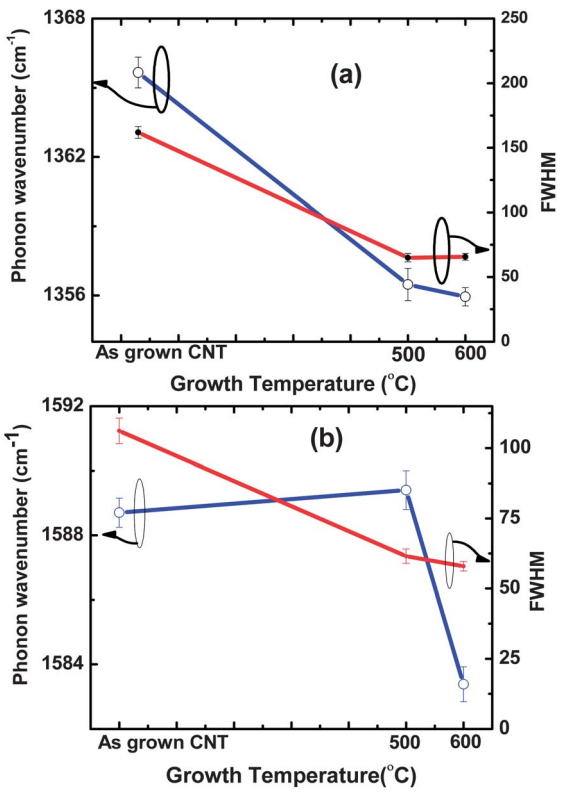

Fig. 6 Depiction of phonon fitting of the high frequency PZT/MWCNT/n-Si hybrid structures, (a) D band (b) G band with different coating temperatures.

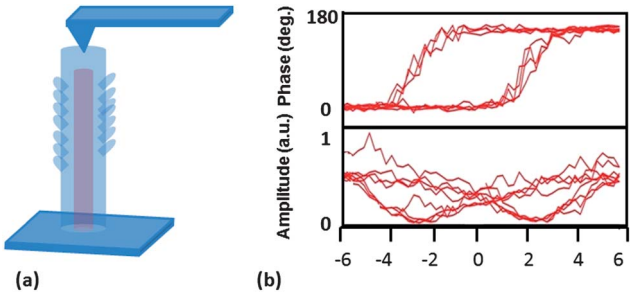

Fig. 7 Phase and amplitude PFM image of switchable ferroelectric PZT on CNT, (a) schematic diagram, (b) piezoelectric hysteresis and butterfly loops.

temperatures. Fig. 6(a) and (b) shows the phonon intensity and full width at half maximum (FWHM) as functions of growth temperature. A significant shift in D-band and G-band towards lower frequencies was observed with increase in the growth temperature of PZT, suggesting three-dimensional stress across the nanostructure due to the conformal coating. The high-frequency G band of hybrid structures grown at 600 °C fit a two-mode model; the higher frequency at 1617 ($\pm$1) cm^{-1} indicates the damage done on the outer layer of MWCNT at high temperature. The high-frequency G-band represents an impure phase of MWCNT. FWHM also narrowed down after deposition of PZT thin films on MWCNTs. Defect peak (D-band) intensity increases with increase in deposition temperature, suggesting possible oxidation of carbon nanotubes above 650 °C. Raman spectra verify the existence of MWCNT and the conformal deposition of functional monoclinic ferroelectric PZT phase. To check the ferroelectric and piezoelectric properties of PZT/MWCNT/n-Si nanostructures, a local piezo force microscopy (PFM) study was carried out over a large area on individual hybrid nanostructures (see schematic diagram Fig. 7(a)).[26,27] Fig. 7(b) shows a typical piezoelectric phase hysteresis loop and butterfly amplitude of PZT/MWCNT hybrid nanostructure. The PFM hysteresis loops were obtained on various individual nanotubes, suggesting well defined ferroelectric switching, however the voltage required for switching of each individual nanotubes shows a significant variation over the large scanning area. Strong switchable PFM signals also validate the coating of ferroelectric PZT monoclinic-rich phase on MWCNT.

Conclusions

In summary, HRTEM studies indicate the formation of nano-sized crystal beads across the cage of the upper layer of PZT having a high dynamic response. *In situ* microstructure indicates that crystal planes, orientations and positions change with interaction of e-beams. This dynamic behavior may be due to the development of localized thermal energy or charge accumulation. The Raman spectra indicate that it is feasible to cover conformally the MWCNT by functional oxide thin films up to 650 °C. Raman spectra and PFM data also verify the formation of a highly functional monoclinic ferroelectric PZT phase on MWCNTs. The observation of a low-lying vibrational mode indicates the presence of nanosize crystals and chemical inhomogeneity in the hybrid structure. These observations suggest that ferroelectric–CNT hybrid structure devices can be fabricated at high temperature.

Acknowledgements

A.K. would like to thank Dr Margarita Correa & Mr Oscar Resto for acquiring the HRTEM data and Sai G. Shivareddy and Prof. Gehan A. J. Amaratunga for providing the aligned MWCNT. A.K. is grateful to Prof. A Gruverman for PFM study.

References

1 D. Eder, Carbon Nanotube–Inorganic Hybrids, *Chem. Rev.*, 2010, **110**, 1348.
2 G. E. Moore, *Electronics*, 1965, **38**(8), 114.
3 P. K. Bondyopadhyay, *Proc. IEEE*, 1998, **86**(1), 78–81.
4 http://www.itrs.net/Links/2010ITRS/2010Update/ToPost/ERD_ERM_2010FINALReportMemoryAssessment_ITRS.pdf.
5 J. R. Powell, *Proc. IEEE*, 2008, **96**(8), 1247.
6 S. Kawasaki, G. Catalan, H. J. Fan, M. M. Saad, J. M. Gregg, M. A. Correa-Duarte, J. Rybczynski, F. D. Morrison, T. Tatsuta, O. Tsuji and J. F. Scott, *Appl. Phys. Lett.*, 2008, **92**, 053109.
7 A. Kumar, S. G. Shivareddy, M. Correa, O. Resto, Y. Choi, M. Cole, R. S. Katiyar, J. F. Scott, G. A. Amaratunga and H. Lu, *Nanotechnology*, 2012, **23**, 165702.
8 S. Iijima, *Nature*, 1991, **354**, 56.
9 A. K. Geim and K. S. Novoselov, *Nat. Mater.*, 2007, **6**(3), 183.
10 Y. Awano, S. Sato, M. Nihei, T. Sakai, Y. Ohno and T. Mizutani, *Proc. IEEE*, 2010, **98**, 2015.
11 J. F. Scott and C. A. P. Araujo, *Science*, 1989, **246**, 1400.
12 T. W. Ebbesen, *Annu. Rev. Mater. Sci.*, 1994, **24**, 235.
13 M. Kumar, V. N. Singh, B. R. Mehta and J. P. Singh, *J. Phys. Chem. C*, 2010, **114**, 2891.
14 M. Kumar, V. N. Singh, B. R. Mehta, N. Koratkar and J. P. Singh, *Mater. Lett.*, 2012, **68**, 47.
15 W. H. Knechtel, G. S. Düsberg, W. J. Blau, E. Hernández and A. Rudio, *Appl. Phys. Lett.*, 1998, **73**, 1961.
16 S. S. Bhattacharyya, G. H. Yang, W. Tie, Y. H. Lee and S. H. Lee, *Phys. Chem. Chem. Phys.*, 2011, **13**, 20435.
17 Y. Choi, L. E. Mosley, Y. Min and G. A. J. Amaratunga, *Diamond Relat. Mater.*, 2011, **19**, 221.
18 N. Ortega, A. Kumar, P. Bhattacharya, S. B. Majumder and R. S. Katiyar, *Phys. Rev. B: Condens. Matter Mater. Phys.*, 2008, **77**, 014111.
19 P. M. Ajayan, T. W. Ebbesen, T. Ichihashi, S. Iijima, K. Tanigaki and H. Hiura, *Nature*, 1993, **362**, 522.
20 D. B. Williams and C. B. Carter, *Transmission Electron Microscopy*, Plenum, New York, 1996.
21 M. Correa, A. Kumar, S. Priya, R. S. Katiyar and J. F. Scott, *Phys. Rev. B: Condens. Matter Mater. Phys.*, 2011, **83**, 014302.
22 R. S. Katiyar, J. F. Ryan and J. F. Scott, *Phys. Rev. B: Condens. Matter Mater. Phys.*, 1971, **4**, 2635.
23 H. B. Zhang, G. D. Lin, Z. H. Zhou, X. Dong and T. Chen, *Carbon*, 2002, **40**, 2429.

24 B. Noheda, D. E. Cox, G. Shirane, J. A. Gonzalo, S. E. Park and L. E. Cross, *Appl. Phys. Lett.*, 1999, **74**, 2059.
25 B. Noheda, J. A. Gonzalo, L. E. Cross, R. Guo, S.-E. Park, D. E. Cox and G. Shirane, *Phys. Rev. B: Condens. Matter Mater. Phys.*, 2000, **61**, 8687.
26 A. Gruverman and A. Kholkin, Nanoscale ferroelectrics: processing, characterization and future trends, *Rep. Prog. Phys.*, 2006, **69**, 2443–2474.
27 M. Alexe and A. Gruverman, *Ferroelectrics at Nanoscale: Scanning Probe Microscopy Approach*, ed. M. Alexe and A. Gruverman, Springer, Berlin, 2004.